

# Experimental study of the Richtmyer-Meshkov instability of a diffuse interface

J.W. Jacobs, B.D. Collins

Department of Aerospace & Mechanical Engineering, University of Arizona, Tucson, AZ 85721, USA

**Abstract:** Previous Richtmyer-Meshkov instability experiments carried out in shock tubes have been hampered by the need to initially separate the two gases with a thin plastic membrane. As a result, these experiments have not been suitable for the use of modern diagnostic techniques such as Planar Laser Induced Fluorescence (PLIF). Furthermore, many of these experiments have had poor agreement with linear stability theory. This limitation has been removed in the present investigation by the use of a novel technique in which the interface is formed by flowing a light and a heavy gas from opposite ends of a vertical shock tube. Both gases exit the shock tube through slots in the test section walls leaving behind a flat interface which is then given a sinusoidal initial shape by gently oscillating the shock tube at a prescribed frequency in the horizontal direction. PLIF has been implemented in these experiments yielding very clear views of the developing instability. In addition, amplitude measurements obtained from these experiments are found to be in excellent agreement with incompressible linear stability theory.

**Key words:** Richtmyer-Meshkov instability, Shock tube experiments

## 1. Introduction

Richtmyer-Meshkov (RM) instability is a very fundamental fluid instability which is of importance to applications ranging from astrophysics to supersonic combustion, yet there is a scarcity of well visualized experimental results. Probably the most significant reason for this deficiency is that RM experiments are typically carried out in shock tubes in which the generation of a sharp well controlled interface between gases is extremely difficult. One approach to this problem has been to use a thin membrane to initially separate the two gases [Meshkov (1969), Benjamin (1988), Aleshin et al. (1988)]. However, the effects of the membrane on the developing instability are significant and impossible to predict. As a result, these studies have found difficulty in achieving initial growth rates that are comparable to that of the linear stability theory of Richtmyer (1960). Furthermore, the presence of broken membrane fragments impedes schlieren or shadowgraph visual-

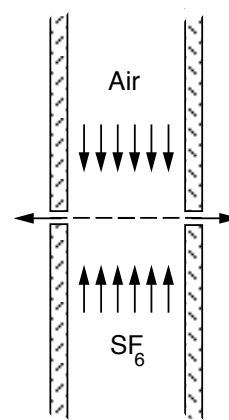


**Figure 1.** The interface-forming flow configuration.

ization, and prohibits the use of more sophisticated visualization techniques such as Planar Laser Induced Fluorescence (PLIF). In attempts to avoid the effects of membranes, other researchers have utilized a solid barrier to initially separate the gases which is then removed immediately prior to firing the shock tube [Brouillette and Sturtevant (1994), Cavailler et al. (1990), Bonazza and Sturtevant (1996)]. However, because the disturbance produced by removing the barrier is normally used as the source of the initial perturbation, these experiments have initial conditions which are nonuniform and difficult to characterize, further complicating comparisons with other experimental and computational studies.

In this paper we present experiments that utilize a new technique [Jones and Jacobs (1997)] whereby a flat, membraneless interface between two gases can be easily generated in a vertical shock tube. This technique makes use of a flow system in which a light gas (Air) and a heavy gas ( $\text{SF}_6$ ) flow from opposite ends of the shock tube driven section. The gases meet and are allowed to exit the tube through slots in the shock tube wall thus forming a stagnation point flow at the interface location (Fig. 1). Relatively low flow velocities ( $\approx 1$  cm/s) combined with a large density ratio ( $\approx 5$ ) produce a very flat and stable (although slightly diffuse) interface in the test section of the shock tube. A sinusoidal perturbation can then be given to this interface by gently oscillating the shock tube in the horizon-

tal direction to produce standing waves. This system, which produces a particularly well defined initial perturbation, has been implemented in shock tube experiments which utilize PLIF flow visualization. Images from these experiments yield very clear views of the instability that show excellent agreement with Richtmyer's linear stability theory.

## 2. Experimental Apparatus

The experiments utilize a vertical shock tube (Fig. 2) which is 4.3 m long and has a 1 m long, 10.2 cm diameter driver, and a 3.3 m long driven section with a 8.9 cm square cross-section. The driver is made of glass fiber wound epoxy pipe, and the upper portion of the driven section is made of extruded fiberglass structural tubing. Thus the shock tube is very light in weight, yet it can withstand pressures resulting from shock Mach numbers up to 1.3. Three walls of the test section are made of flat black anodized aluminum while the fourth wall is transparent acrylic sheet to allow full optical access for flow visualization.

An interface is formed in the test section using the technique described above whereby a heavy gas ( $\text{SF}_6$ ) flows upward in the shock tube and collides with a light gas (Air) flowing downward. The light gas enters through a plenum at the top of the driven section immediately below the diaphragm, and the heavy gas enters through a similar plenum at the bottom of the test section. Both gases exit the shock tube through slots in the test section wall, leaving behind a flat stable interface. The shock tube is mounted by pins at its upper end so that it can be pivoted in the horizontal direction. A sinusoidal initial shape is then given to the interface by oscillating the shock tube in the horizontal direction using a stepper motor and crank mechanism. A weak shock wave ( $M_s = 1.1$ ) is generated by puncturing a polypropylene diaphragm which travels down the tube where it impacts the interface to produce the instability. The firing of the shock tube is synchronized with the motion of the stepper motor to achieve repeatable initial perturbations.

The flow is visualized in these experiments utilizing Planar Laser Induced Fluorescence (PLIF). The light gas is seeded with nearly saturated acetone vapor and illuminated by the fourth harmonic (266 nm) of a pulsed Nd:YAG laser positioned at the lower end of the shock tube. The laser's output is passed through circular and cylindrical lenses and reflected upward through a window in the shock tube end wall producing a light sheet that illuminates a thin ( $\approx 1$  mm) cross section of the interface. The resulting fluorescent image is captured by a thermoelectrically cooled CCD camera. The low repetition rate of the laser precludes the capturing of more than one image of the interface

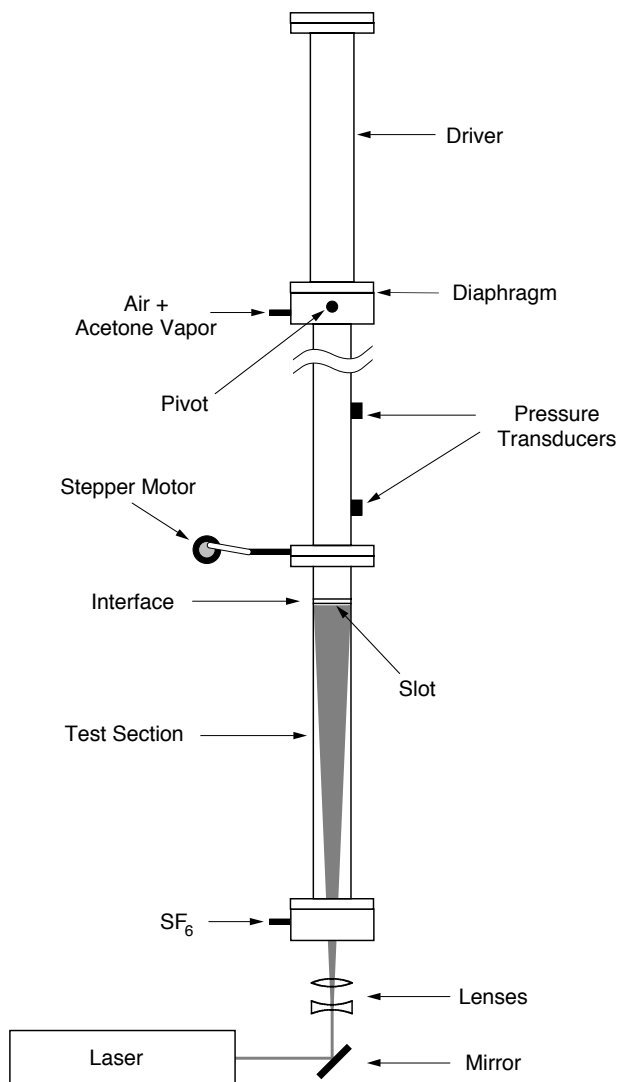
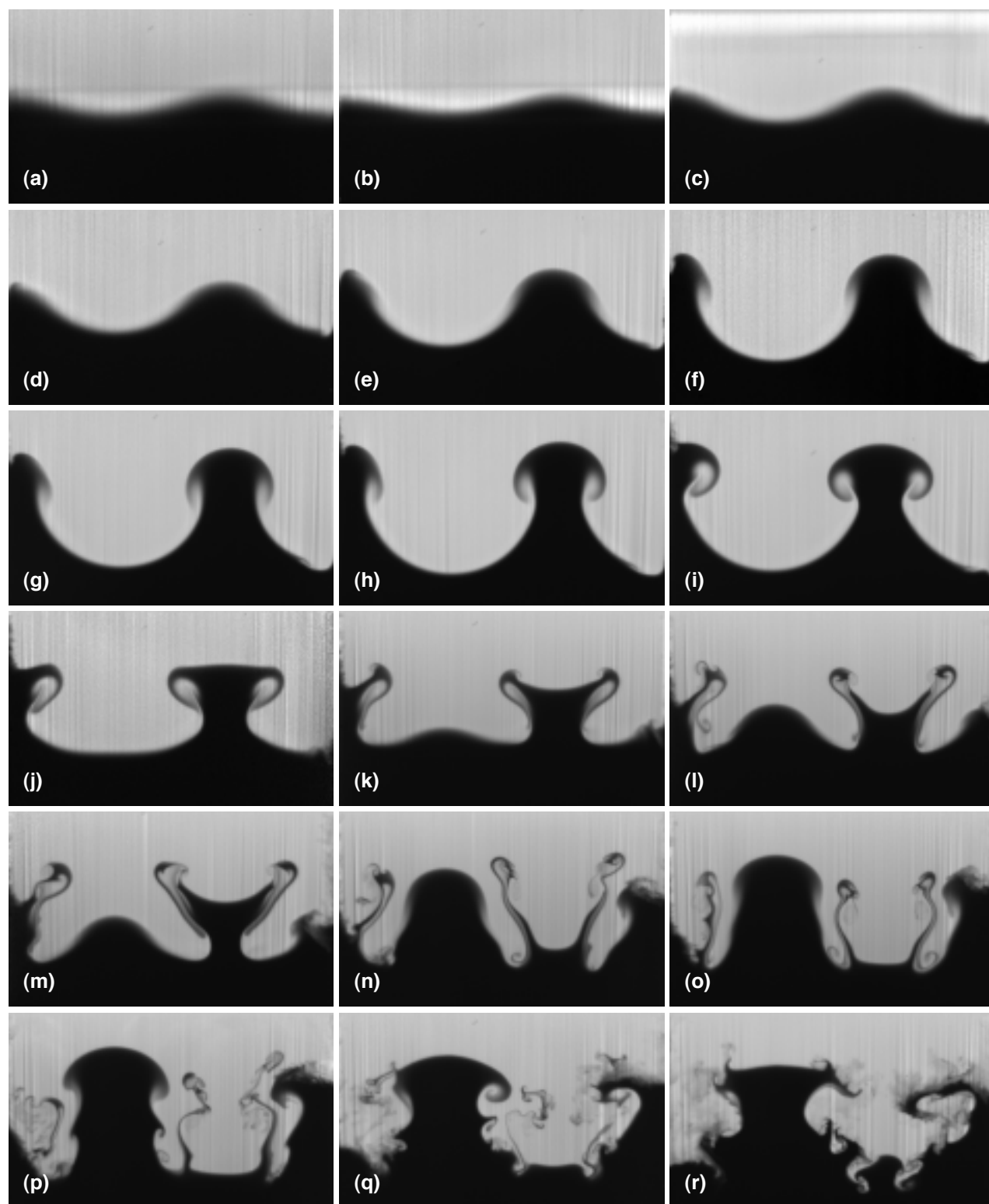


Figure 2. The shock tube and PLIF system.

per experiment. The single laser pulse is triggered by the passage of the shock wave over a pressure transducer mounted in the shock tube wall above the interface. The trigger signal is then delayed to produce the desired time of capture. Time sequences are then generated by multiple shock tube firings utilizing different delay times and camera positions.

The absorption of the incident laser light is very strong for the relatively high concentrations of acetone used in this study. Therefore, the captured PLIF images must be corrected to obtain realistic concentration distributions. The captured images were corrected by integrating Beer's law along individual light rays. The system is calibrated and the extinction coefficient is computed by assuming that regions far above the interface contain a uniform known concentration of acetone.



**Figure 3.** Corrected PLIF images assembled to form a time sequence. The lighter (upper) gas has been seeded with acetone vapor, and the laser light enters from below. Frame (a) was taken slightly before the arrival of the shock wave. Times relative to the shock arrival for the other photographs are: (b) 0.018 ms, (c) 0.607 ms, (d) 1.212 ms, (e) 2.207 ms, (f) 3.217 ms, (g) 4.215 ms, (h) 5.204 ms, (i) 6.221 ms, (j) 7.026 ms, (k) 7.546 ms, (l) 8.027 ms, (m) 8.535 ms, (n) 8.804 ms, (o) 9.054 ms, (p) 9.555 ms, (q) 10.053 ms, (r) 10.558 ms. A reflected expansion reaccelerates the interface beginning between frames (h) and (i) and a weakened reflected shock impacts the interface in frame (p).

### 3. Results and discussion

Figure 3 is a sequence of PLIF images showing the evolution of the instability in these experiments. Recall that only one picture can be acquired per experiment; therefore, this sequence was assembled from 18 separate experiments. Figure 3(a) was taken slightly before the arrival of the shock wave and thus represents the initial perturbation and Fig. 3(b) was taken slightly after the shock had passed over the interface (at  $t = 0.018$  ms). In comparing Figs. 3(a) and (b), one can observe the effects of the compression produced by the incident shock wave to reduce both the perturbation amplitude and the interface thickness. Initially, the instability retains its sinusoidal shape, developing primarily by increasing amplitude [Fig. 3(c)]. At later times, the interface becomes significantly nonsinusoidal with the appearances of mushroom structures, produced by the coalescence of the baroclinic vorticity initially deposited on the interface by the shock wave [Figs. 3(f) – 3(h)]. Note that this relatively high Atwood number instability (preshock Atwood number = 0.604) shows considerable top-to-bottom asymmetry, exhibiting more of the bubble and spike configuration characteristic of a large Atwood number instability.

The interface is reaccelerated in the opposite direction beginning at  $t \approx 6$  ms by the expansion wave which originates at the diaphragm location and subsequently reflects off of the top end of the shock tube. This interaction initially causes the amplitude to decrease slightly [in Figs. 3(i) and (j)] In addition, one can observe the appearance of opposite signed vorticity on the mushroom stems. Eventually, the interaction causes the entire interface to invert producing wave crests where there once were troughs and troughs where there were crests. This process is accompanied by a dramatic increase in complexity and ultimately results in a flow that appears to be turbulent. Note that the expansion wave acts on an interface which has significantly steeper slopes than that of the initial perturbation. Thus, much more vorticity is produced by the interaction with the expansion than was produced in the initial shock interaction. The interface is again accelerated [in Fig. 3(p)] by the remnants of the original incident shock wave that has been reflected off of the bottom of the shock tube. However, the reflected shock has been significantly weakened by the interaction with the earlier arriving expansion wave. Therefore, its effects are minimal.

Figure 4 is a plot of the mean displacement of the interface (up until the interaction with the expansion) relative to its initial position in the shock tube for 55 experiments. This data was obtained by measuring the distances traveled by the centermost

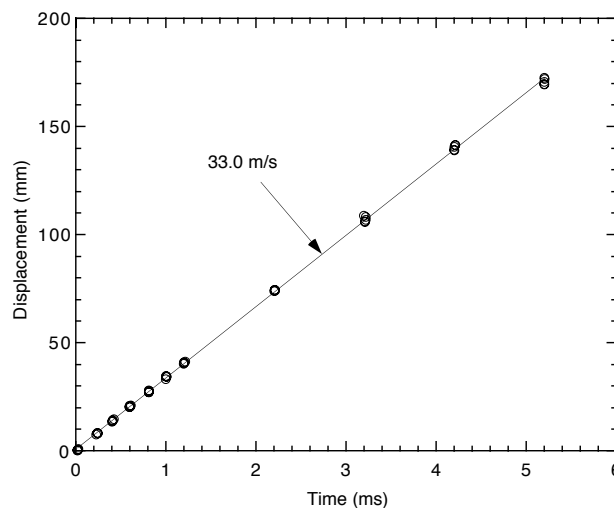


**Figure 4.** Plot of the displacement of the interface from its initial position. The solid line is a curve fit of the data giving an interface velocity of 33.0 m/s.

crest and trough in the PLIF images, and then averaging these to obtain the mean interface position. The data indicate a nearly constant velocity of approximately 33 m/s until the point of reacceleration by the reflected expansion (at  $t \approx 6$  ms). Remarkably, the velocity remains constant despite the fact that the shock tube contains two large holes (i.e., the slots). However, it should be noted that the theoretically expected value of interface velocity, calculated by considering the transmission of the shock wave through a flat Air/SF<sub>6</sub> interface (without slots), is 36 m/s. Therefore, the presence of holes has apparently produced a slight decrease in the interface velocity.

The growth in the amplitude of the interface for the experiments plotted in Fig. 4, found by taking the difference in the measured crest and trough displacements and dividing by two, is shown in Fig. 5. The initial data at  $t \approx 0$  were taken at a time corresponding to the point where the shock wave has just passed over the interface [i.e., Fig. 3(b)]. Therefore these values represent the postshock amplitude. The data in this figure exhibit significantly more scatter than the displacement data, caused by small run-to-run variations in the initial amplitude. However, one can easily observe that the amplitude increases nearly linearly until  $t \approx 2$  ms. At  $t \approx 5$  ms, the growth has slowed, and at  $t \approx 6$  ms, reacceleration has caused the amplitude to decrease slightly.

Because the initial amplitude is relatively small in these experiments (wavenumber  $\times$  amplitude  $\approx 0.2$ ), one would expect linear stability theory to apply. Richtmyer (1960) modeled the instability by considering an impulsively accelerated incompressible system

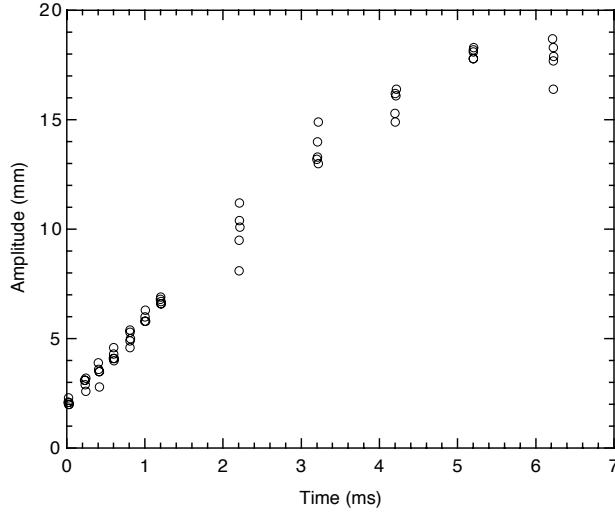


**Figure 5.** Plot of instability amplitude versus time. The initial data at  $t \approx 0$  were taken at a time corresponding to the point where the shock has just passed over the interface.

and found the growth rate to be given by

$$\frac{da}{dt} = kAVa_0 \quad (1)$$

where  $a_0$  and  $k$  are the amplitude and wavenumber of the initial perturbation,  $V$  is the change in the velocity produced by the impulsive acceleration (which in this case should equal the interface velocity), and  $A$  is the Atwood number defined by

$$A = \frac{\rho_2 - \rho_1}{\rho_2 + \rho_1} \quad (2)$$

In this case  $\rho_1$  and  $\rho_2$  are the densities of the air/acetone mixture and  $\text{SF}_6$ , respectively. Richtmyer recognized that the values of both the initial amplitude and the Atwood number will change during the shock interaction process due to shock compression. Thus he used comparisons with numerical simulations to conclude that the use of the postshock values provide the best growth rate estimates for interactions which result in the generation of a reflected shock wave (i.e., light-heavy configurations such as in the present experiment).

Richtmyer's analysis assumes that the fluids are separated by a sharp, i.e., discontinuous, interface. Brouillette and Sturtevant (1994) modeled the diffuse instability by extending the analysis of the Rayleigh-Taylor instability of a diffuse interface by Duff et al. (1962), and found the growth rate of a diffuse Richtmyer-Meshkov system to be given by,

$$\frac{da}{dt} = \frac{kAV}{\Psi} a_0 \quad (3)$$

where  $\Psi$  is a growth reduction factor which is determined as the eigenvalue of the Sturm-Liouville bound-

ary value problem:

$$\frac{1}{\rho} \left( \rho \frac{df}{dy} \right) - \left( 1 - \frac{\Psi}{kA} \frac{1}{\rho} \frac{d\rho}{dy} \right) k^2 f = 0 \quad (4)$$

$$f \rightarrow 0 \quad \text{as } y \rightarrow \pm\infty$$

Note that  $\Psi$  equals 1 for a discontinuous interface and increases monotonically with increasing interface thickness. Integrating (3) to obtain the time dependence of the amplitude yields

$$a(t) = a_0 \left( 1 + \frac{kAV}{\Psi} t \right) \quad (5)$$

The density distribution in (4) was approximated by fitting an error function to the postshock acetone concentration distribution (which yielded a maximum slope thickness of 3.7 mm) and using values of the wavenumber and Atwood number measured from the present experiments. The resulting solution of (4) yields a value of  $\Psi = 1.132$ . Thus in this case an interface thickness of approximately 6% of the perturbation wavelength, reduces the growth rate by 12%. Evaluating (3) using this value of  $\Psi$  along with the estimated postshock Atwood number, and measured values of the wavenumber, interface velocity, and the postshock amplitude yields a growth rate of 3.99 m/s.

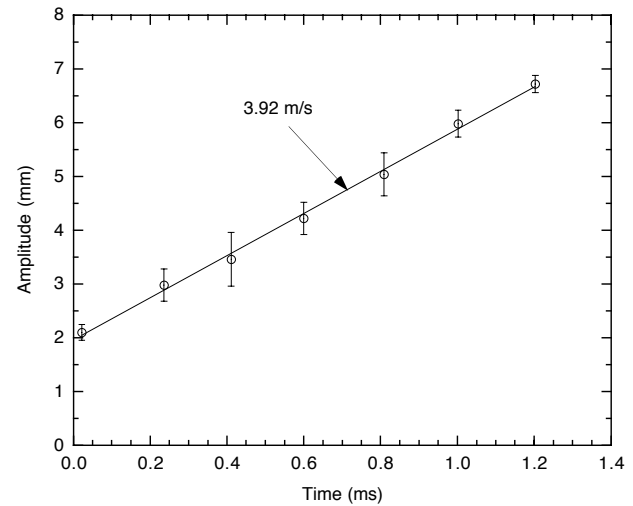


**Figure 6.** Plot of the early time amplitude versus time. The symbols represent the mean values at each time level and the error bars correspond to the associated 95% confidence intervals. The solid line is a curve fit of the data giving a growth rate of 3.92 m/s.

Figure 6 shows mean values of the early time amplitude data of Fig. 5. Note that there are five amplitude measurements for every time level shown in Fig. 5. Therefore, the symbols in Fig. 6 represent the mean value of each set of five measurements and the error bars represent the associated 95% confidence intervals.

The solid line shown on this plot is a linear curve fit of the data which has a slope of 3.92 m/s. Thus, the growth rate measured from the experiments is within 2% of that predicted by Eq. (3) above. It is interesting to note that using the preshock values of the amplitude, Atwood number and  $\Psi$  to evaluate (3) yields a measured growth rate of 4.02 m/s which is in only slightly worse agreement than that predicted by the postshock conditions. The closeness of the two estimates is a result of the fact that the shock compression decreases both the initial amplitude and the interface thickness. A decrease in the amplitude results in a decrease in the growth rate; however a decrease in the interface thickness produces an increase in the growth rate. Thus, the two effects effectively cancel each other resulting in an almost negligible change in the predicted growth rate. Therefore, as Richtmyer similarly found, the post shock amplitude provides the better growth rate estimate. However, the difference between the pre and postshock values is very small.

#### 4. Conclusions

We have carried out RM instability shock tube experiments utilizing a new technique for generating a well characterized interface between two gases. PLIF images obtained from these experiments show very clearly the development of the instability from a sinusoidal perturbation far into the nonlinear regime, including the formation of bubbles and spikes, and the development of vortices. Early-time measurements of the amplitude of the unstable interface show excellent agreement with the incompressible model of Richtmyer (1960) when combined with the extension of this model by Brouillette and Sturtevant (1994). This agreement, which is much better than that reported in previous experiments, demonstrates the applicability of Richtmyer's incompressible model for the weak shock strengths and small initial amplitudes considered here. Furthermore, it suggests that the large degree of disagreement between Richtmyer's model and previous experiments may have been caused by the strength of the membranes used to initially separate the gases in these studies.

**Acknowledgement.** This research was supported by Lawrence Livermore National Laboratory through CAFDA and by NASA's Microgravity Fluid Physics program.

#### References

Aleshin AN, Gamalii EG, Zaitsev SG, Lazareva EV, Lebo IG, Rozanov VB (1988) Nonlinear and transitional states in the onset of the Richtmyer-Meshkov instability. *Sov. Tech. Phys. Lett.* 14:466–468.

Benjamin RF (1988) Experimental observations of shock stability and shock-induced turbulence. *Proc. 1st Intl. Workshop on the Physics of Compressible Turbulent Mixing*, 24-27 October 1988, Princeton, NJ: 341–348.

Bonazza R, Sturtevant B (1996) X-ray measurements of growth rates at a gas interface accelerated by shock waves. *Phys. Fluids* 8:2496–2512.

Brouillette M, Sturtevant B (1994) Experiments on the Richtmyer-Meshkov instability: single-scale perturbations on a continuous interface. *J. Fluid Mech.* 263:271–292.

Cavailler C, Mercier P, Rodriguez G, Haas JF (1990) A new vertical shock tube for Rayleigh-Taylor instability measurements. *Proceedings of the 17th International Symposium on Shock Waves*: 564

Duff RE, Harlow FH, Hirt CW (1962) Effects of diffusion on interface instability between gases. *Phys. Fluids* 5:417–425.

Jones MA, Jacobs JW (1997) A membraneless experiment for the study of Richtmyer-Meshkov instability of a shock-accelerated gas interface. *Phys. Fluids* 9:3078–3085.

Meshkov EE (1969) Instability of the interface of two gases accelerated by a shock wave. *Izv. Akad. Nauk. SSSR Mekh. Zhidk. Gaza* 4:151–157.

Richtmyer RD (1960) Taylor instability in shock acceleration of compressible fluids. *Commun. Pure Appl. Math.* 23:297–319.